Proceedings of the 2009 IEEE International Conference on Systems, Man, and Cybernetics
San Antonio, TX, USA - October 2009

# The Design of Wireless Sleep EEG Measurement System With Asynchronous Pervasive Sensing

Ming-Feng Wu[1,2]
[1]Division of Chest Medicine
Taichung Veterans General Hospital
Taichung 407, Taiwan, R.O.C.
{osmigo@seed.net.tw}

Chih-Yu Wen[2]
[2]Department of Electrical Engineering/GICE
National Chung Hsing University
Taichung 402, Taiwan, R.O.C.
{cwen@dragon.nchu.edu.tw}

***Abstract*—The Electroencephalogram (EEG) signals reflect local potential changes that occur on pyramidal cell. Based on the received signals, epileptic seizure and sleep patterns can be monitored and diagnosed. This paper proposes an asynchronous pervasive sensing method using cooperative communication and networking between a pair of sensors for wireless sleep EEG signal collection. A theoretical analysis and experiments are developed to assess the impact of time synchronization errors and the performance of the proposed approach, which may provide a sensible way for practical system design.**

***Index Terms*—wireless sensor networks; sleep EEG system.**

## I. Introduction

Electroencephalogram (EEG) is widely used to diagnose epileptic seizure, consciousness, drug control and sleep patterns [1]. It represents a visual description of brain electrical activity obtained through arrays of electrodes placed across the scalp [2]. The results in electrical activity come from the extra cellular flow of current associated with summated excitatory postsynaptic potentials and inhibitory postsynaptic potentials. The waveforms are displayed and recorded by means of an amplifier with potential differences like a typical half-cell potential at different points [3].

Physiological bio-potential signals (e.g., EEG and electrocardiogram (ECG) data) are often corrupted by frequency interference. As a result, the bio-potential measurement systems are typically designed with wire systems. Recently, wireless technologies are used for medical applications, which are more intimate to the subjects compared with wire ones. For instance, a multi-channel wireless EEG system is developed in [4], which includes a sensing unit, a transmission unit, and a digital processing circuit.

In this work, a design of wireless sleep EEG measurement system with asynchronous pervasive sensing is proposed. Generally, International 10-20 system is applied for monitoring full complement EEG electrode activity. The standard sleep EEG recordings are $C_4$-$A_1$, $C_3$-$A_2$, $O_1$-$A_2$, or $O_2$-$A_1$ [5]. In our design, a bipolar measurement (i.e. the potential difference between neighboring electrodes) is used. A pair of sensor nodes and a sink work as a group for signal collection. Here, we take $C_4$-$A_1$ as two local sleep EEG activities for presenting signal transmission. Assume that $C_4$ is primary point and $A_1$ is secondary point. Each sensor node consists of a sensor lead, a preamplifier, and a wireless transceiver. The sink is responsible for signal storage, analysis, and display.

In a standard wire/wireless sleep EEG system, by having one single signal collection unit, the cables may be running over the head and a single wireless transmission unit would be needed without time synchronization problem. In contrast, we propose a pure wireless-based sleep EEG measurement system to get rid of any cables running to the electrodes attached to the scalp $C_4$ and the ear $A_1$. Therefore, each of the nodes would need a separate wireless transmission unit and synchronization effort would be required. Since time synchronization is important for network operation in sensor networks [6], it is necessary to consider time calibration problem between $A_1$ and $C_4$ and the message transfer delay during the signal collection process. Moreover, in order to diagnose the signal correctly, proper signal segmentation principles are essential for the sink to interpret the received signals. To this end, the *Asynchronous Pervasive Sensing Algorithm* (APSA) executes the sleep EEG signal collection in two phases: (I) Time Synchronization and Signal Collection and (II) EEG Signal Segmentation.

In Phase I, bidirectional communication between a pair of sensors provides an opportunity to invoke a calibration step (e.g. timing calibration) and employ techniques to adjust the variations in transceiver characteristics (e.g. correct latencies induced by system components) within the estimation procedures. That is, pairs of sensors can measure the message transfer delay through bidirectional communication and information sharing to improve measurement accuracy in a low-precision environment without synchronous clocking.

Once the signal is collected, interpretation of the received signal becomes an issue. In order to govern different sleep EEG patterns efficiently, in Phase II a signal segmentation scheme is applied, especially on the changes in the spectral character of signals.

The proposed solution integrates time synchronization and information processing to complete joint distributed synchronization and signal classification with cooperative communications. Compared with conventional EEG signal collection techniques such as [7], the proposed algorithm simultaneously undertake time synchronization and the estimation of signal arrival time such that a reliable sleep EEG reading system can be provided with asynchronous pervasive sensing.

The organization of this paper is as follows: Section II reviews the current literature on wireless EEG signal collection. Section III describes the design principles and the proposed



978-1-4244-2794-9/09/$25.00 ©2009 IEEE

algorithm. In Section IV, an analytical tool is built up to approximate the desired performance of the proposed scheme. Section V illustrates the simulation results and summarizes the performance of the proposed methodology. Finally, Section VI draws conclusions and shows future research directions.

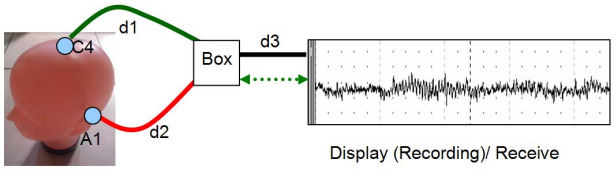


Fig. 1. Overview of a standard wire/wireless EEG system, where the Box consists of a preamplifier and a filter.

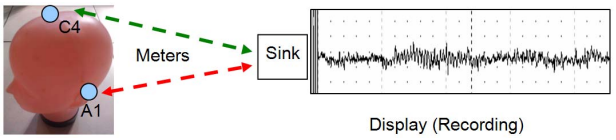


Fig. 2. Each sensor node transmits bio-potential signals to the Sink.

## II. Literature Review

[8] designs and tests a prototype portable EEG system. It consists of input instrumentation amplifier, band-pass filter, driven-right-leg circuit and analog digital converter. [9] develops wireless technologies for medical application. Based on wireless network protocols, the wireless transmission pathways for portable and long time recording. Figure 1 depicts the standards overview of a wire/wireless EEG system. [10] presents a design of a hybrid medical sensor network with Tmote Sky motes as wireless EEG sensor nodes and uses Independent Component Analysis (ICA) to remove artifacts and then to analyze with a Fourier transformation.

As illustrated in Figure 2, Ng [7] designs a wireless programmable system for bio-potential signal acquisition, including a base unit and a plurality of individual wireless, remotely programmable transceivers that connect to patch electrodes. The base unit manages the transceivers by issuing registration, configuration, data acquisition, and transmission commands using wireless techniques. [4] proposes a multi-channel wireless EEG system, which allows the signal to be observed and stored without any long cables and further analyzed by an integrated classification method. However, preamble concepts and synchronization techniques are implemented in each wireless channel without considering wireless transmission effects, which may substantially degrade the EEG signal in the back-end system.

## III. Asynchronous Pervasive Sensing Algorithm

This section describes a distributed algorithm, which applies the concept of cooperative communication and networking to achieve the task of signal collection efficiently. Figure 3 shows the system architecture of one-pair mixed sleep EEG for the proposed scheme. The procedures of the proposed algorithm are described in the following subsections.

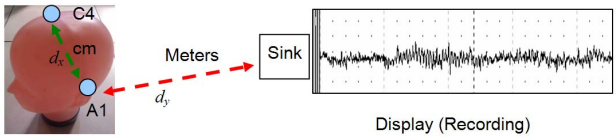


Fig. 3. The architecture of the proposed sleep EEG system.

### A. Phase I: Time Synchronization and Signal Collection

*1) Overview of Time Calibration Method:* In order to synthesize a signal, a distributed time calibration method [11], based on a two-way time-of-arrival approach, may be used to simultaneously undertake synchronization and propagation time estimation. It operates analogously to a pulsed radar in which a signal is bounced from the target and the propagation time is determined by how long it takes the signal to return. Since sensors are typically small and operate with low power; the signal cannot bounce from the receiver. Instead, the target sensor receives the transmission and sends a reply that acts analogously to the return of the radar. Moreover, this method helps to alleviate the need for highly accurate synchronous clocking. Suppose that sensors A and B are equipped with clocks (oscillators) that are assumed to be asynchronous in both frequency and phase. Denote $t_i^a$ and $t_j^b$ as the time stamps in sensors A and B, respectively; let $t_{del}^a$ and $t_{del}^b$ be the delay time in sensors A and B, respectively; the scale factor $z$ is used for time adjustment, $t_{ab}$ is the signal propagation time. The estimation proceeds as shown in Figure 4.

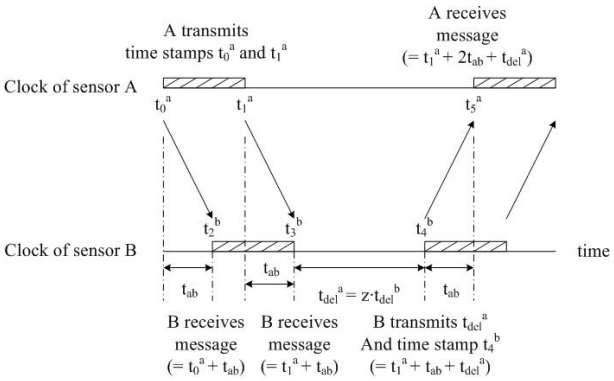


Fig. 4. Time synchronization using the time stamps of transmission and reception in sensors A and B.

In order to alleviate the multipath effect in the wireless channel, the precoding technique, such as Tomlinson-Harashima (TH) precoding [12][13], is used for the propagation time measurement between pairs of sensors. This pre-equalization technique is used principally in data transmission systems to combat the effect of interchannel interference

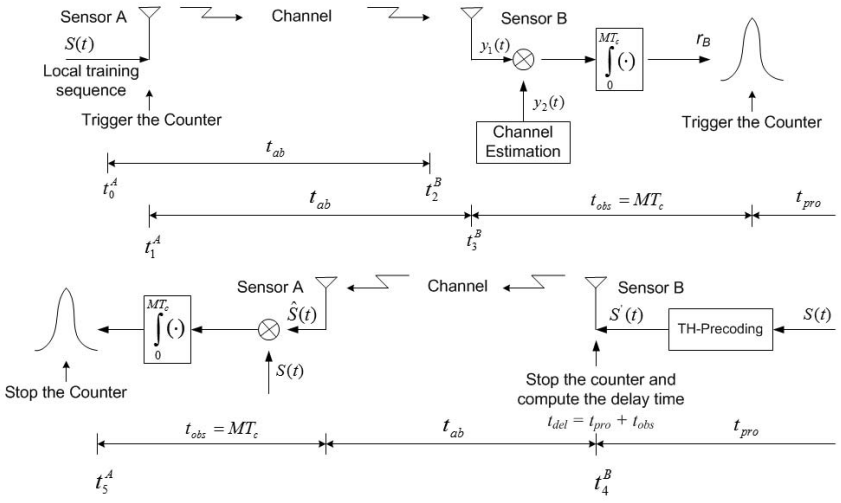


Fig. 5. Block diagram of a bidirectional communication and time measurement system using channel estimation and TH precoding.

caused by channel characteristics, which is crucial to the estimation accuracy of the propagation time. Given two sensors A and B, sensor A initiates communication by sending a training sequence. Then, sensor B carries out a channel estimation based on maximizing the output of the correlator. Based on channel estimation, sensor B generates a modified training sequence for correlating with the training sequence sent from sensor A. Once sensor B detects the peak of the correlator output, it triggers a time counter and initiates the TH precoding. After receiving the signal from sensor B, sensor A stops the timer based on the performance of the correlator output and calculates the propagation time $t_{ab}$. Thus, sensor B estimates the channel and applies the TH precoding using a training sequence sent by sensor A, and allows A to accurately estimate the propagation time.

Build upon the concept of time calibration method and the TH precoding technique, Figure 5 depicts the block diagram of a bidirectional communication and time measurement system using channel estimation and TH precoding. Note that $s(t)$ is the local training sequence, $y_1(t)$ is the received training sequence, $y_2(t)$ is the modified training sequence that can be used to correlate with $y_1(t)$, $r_B(t)$ is the correlator output, $T_c$ represents the time interval between symbols, $MT_c$ is the correlation time, and $t_{pro}$ is the processing delay.

These asynchronous and cooperative communication procedures may simplify the computational and circuitry complexity of the propagation time estimation in each sensor. This method shows that time delay estimation is possible without synchronous clocking. Based on the system architecture in Figure 5, the impact of the precoding technique and the correlation procedure on propagation time estimation is further explored in Section IV.

*2) Signal Collection:* When $A_1$ transmits a message to $C_4$ for triggering the process of signal collection, $C_4$ transmits its detected signal to $A_1$ for producing the desired signal. After that, $A_1$ transmits the mixed signal to the sink for further analysis and classification.

### *B. Phase II: EEG Signal Segmentation*

*1) Overview of Non-Linear Energy Operator:* Assume the input signal $x(n) = A\cos(\omega n + \phi) + w(n)$, where $w(n)$ is AWGN with power $\sigma_w^2$, and A and $\omega$ represent the amplitude and frequency of the input signal, respectively. Considering the following Non-Linear Energy Operator (NLEO) [14]

$$\Psi[x(n)] = x(n-1)^2 - x(n)x(n-2), \tag{1}$$

the expected value of the output for $x(n)$ is

$$E[\Psi[A\cos(\omega n + \phi) + w(n)]] \approx A^2\omega^2 + \sigma_w^2, \tag{2}$$

In general, different EEG patterns are distinguished by the dominant rhythms present in the signal, which suggests that the changes in the spectral character of signals may be used to segment EEG signals because of the relative sensitivity in the frequency weighted energy.

*2) Segmentation Criterion:* Since the time instants of energy change correspond to the segmentation boundaries, a sliding temporal window method in [15] may be used to generate the segmentation criterion to detect these changes, where the signal $G_{nleo}(n)$ yields

$$G_{nleo}(n) = \left| \sum_{m=n-N+1}^{n} \Psi(m) - \sum_{m=n+1}^{n+N} \Psi(m) \right|. \tag{3}$$

The method considers the neighborhood of the observed time instant and compares the pre- and post-change frequency weighted energy to detect subtle but clinically important local changes. Moreover, in order to reduce some spurious redundant segment boundaries due to the inherent random fluctuations, an adaptive thresholding procedure is developed to maintain the robustness of the algorithm, which is given by

$$T(n) = \max[G_{nleo}(n - L/2 : n + L/2)], \tag{4}$$

where $n = L/2, (L/2+1), \ldots$. Accordingly, a new segmentation criterion, $G(n)$ can be derived,

$$G(n) = \begin{cases} G_{nleo}(n) & \text{if } G_{nleo}(n) \geq T(n) \\ 0 & \text{if } G_{nleo}(n) < T(n). \end{cases} \quad (5)$$

Thus, final segmentation boundaries can be identified by finding the local maxima or peaks.

Figure 6 illustrates the simulation result using the approach detailed in Section III-B for signal segmentation. Observe that with synchronous clocking and without the signal measurement noise, the segmentation criterion can be applied to separate the test signals successfully.

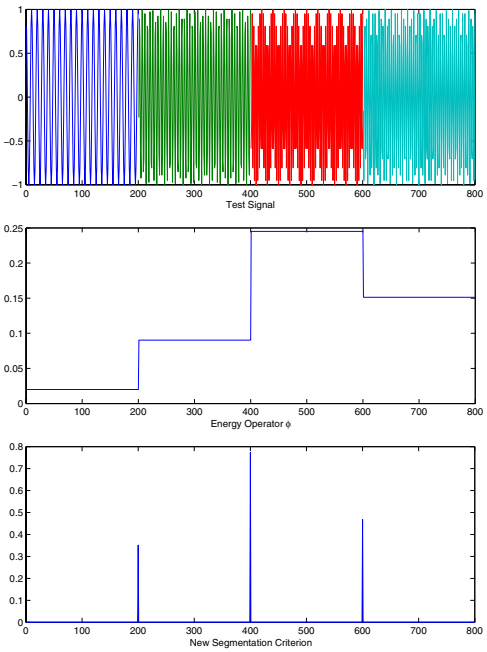


Fig. 6. Simulation example of segmentation of two channels with synchronous clocking and without measurement noises; $f_1 = 5K$ Hz, $f_2 = 2{*}f_1$ Hz, $f_3 = 3.5 * f_1$ Hz, and $f_4 = 2.75 * f_1$ Hz. The sampling frequency $f_s = 10 * f_1$ Hz.

## IV. Analysis

The impact of time synchronization problem and the measurement noise on the performance of the proposed sleep EEG system is explored in this section. The Gaussian approximation is applied to describe the estimation accuracy of propagation time between $C_4$ and $A_1$ and the estimation accuracy of signal segmentation.

### A. Estimation Accuracy of Propagation Time

The fundamental limitation on time accuracy of the propagation time estimate between a pair of sensors, sensors A and B, is related to the form of the signal and the clock, including signal bandwidth, signal-to-noise ratio (SNR), and timing calibration. Assume that the random time error and time bias error from propagation conditions are negligible. The time-measurement accuracy may be characterized by the measurement error

$$\sigma_P = \left(\sigma_S^2 + \sigma_{clock}^2\right)^{1/2}, \quad (6)$$

where $\sigma_S$ is the SNR-dependent random time accuracy and $\sigma_{clock}$ is the clock-dependent random time accuracy. Note that $\sigma_S$ relates the accuracy of synchronous propagation time estimates to the signal-to-noise ratio and the effective bandwidth of the signal. The expression of $\sigma_{clock}$ is the added inaccuracy due to the asynchronous clocking mechanism as detailed in [11].

For the SNR-dependent propagation time measurement, the estimation accuracy is influenced by the error sources such as channel estimation, correlator performance, and signal format. Due to channel estimation errors, sensor B may possess erroneous channel information, which may degrade the performance of the TH precoder. Assume that the channel estimation is assumed to be accurate (i.e. the variance of the correlator is negligible and the proper correlation peak is chosen). Accordingly, the accuracy of synchronous propagation time estimates [16]-[18] is related to the signal-to-noise ratio, the distance, and the effective bandwidth of the signal, which is given by

$$\sigma_S \geq \frac{d_{ab}}{2\beta_e\sqrt{2\text{SNR}}}, \quad (7)$$

where $\beta_e$ is the effective bandwidth of the signal [18].

Now consider sensor *A* and *B* in the above analysis as the primary point ($C_4$) and the secondary point ($A_1$), respectively. Hence, the estimation error of signal propagation time between $A_1$ and $C_4$ in the proposed method is

$$\sigma_P = \left(\sigma_S^2 + \sigma_{clock}^2\right)^{1/2} \geq \sqrt{\frac{d_{ab}^2}{8\beta_e^2\text{SNR}} + \sigma_{T_{ab}}^2}. \quad (8)$$

### B. Estimation Accuracy of Signal Segmentation

This subsection investigates the impact of estimation accuracy of the propagation time on signal segmentation. Based on the messages communicated between $A_1$ and the sink, $A_1$ may estimate the channel and transmit the pre-equalized signal to the sink using the TH-Precoding. Thus, the samples of the received signal at the sink can be denoted as

$$x(n) = A\cos\left(\frac{2\pi f_0}{f_s}n + \phi\right) + w(n) \quad (9)$$

where *A* is the signal amplitude, $f_0$ is the carrier frequency, $f_s$ is the sampling frequency, $\phi$ is the initial phase, and $w(n)$ is AWGN noise. Then based on the Non-Linear Energy Operator as described in (1), the calculation of $x(n-1)^2$ is given by

$$x(n-1)^2 = \frac{A^2}{2} \cdot [f(2n-2) + f(0)] + g(w(\cdot)) \quad (10)$$

where $f(z) = \cos(\Omega_0 \cdot z + \phi_z)$, $g(w(\cdot))$ is a function of AWGN noise, $t_s = 1/f_s$, $\Omega_0 = 2\pi f_0 t_s$, and $\phi_z = 2\pi f_0 \triangle t \cdot z + \phi$. Note that $\triangle t$ is assumed to be a normal random variable with

distribution $\mathcal{N}(0, \sigma^2_{\triangle t})$, which is related to the estimation accuracy of propagation time or the clock measurement accuracy. Similarly, $x(n)x(n-2)$ yields

$$x(n)x(n-2) = \frac{A^2}{2} \cdot [f(2n-2) + f(2)] + g(w(\cdot)). \quad (11)$$

Without loss of generality, let the initial phase $\phi = 0$. Therefore, the resulting output $E[\Psi[x(n)]]$ is

$$E[\Psi[x(n)]] = A^2 \sin(U) \sin(V) + \sigma_w^2 \approx A^2 \cdot U \cdot V + \sigma_w^2 \quad (12)$$

where

$$U = V = \Omega_0 + \frac{\phi_2}{2} \sim \mathcal{N}(2\Omega_0, 4\pi^2 f_0^2 \sigma^2_{\triangle t})$$

Applying the Gaussian approximation derived in [19]-[21], the distribution of $E[\Psi[x(n)]]$ is

$$E[\Psi[x(n)]] \sim N(\mu_U \mu_V, \mu_U^2 \sigma_V^2 + \mu_V^2 \sigma_U^2 + \sigma_w^2). \quad (13)$$

Since the signal measured in the primary point $C_4$ is transmitted to the secondary point $A_1$, $\triangle t$ is related to the estimation accuracy of propagation time. Based on (12), the distribution of the resulting output $E[\Psi[x(n)]]$ of $C_4$ is given by

$$E[\Psi_{C_4}[x(n)]] \sim \mathcal{N}(\mu_{C_4}, \sigma^2_{C_4}), \quad (14)$$

where $\mu_{C_4} = A^2\Omega^2_{C_4}$, $\sigma^2_{C_4} = \Omega^2_{C_4}(\sigma^2_{U(C_4)} + \sigma^2_{V(C_4)}) + \sigma^2_w$, $\sigma^2_{U(C_4)} = \sigma^2_{V(C_4)} = 4\pi^2 f^2_{C_4} \sigma^2_P$, and $\sigma^2_P$ is the propagation time measurement error as described in (8).

For the secondary point $A_1$, $\triangle t$ is related to the clock-dependent time accuracy. The distribution of the resulting output $E[\Psi[x(n)]]$ of $A_1$ is

$$E[\Psi_{A_1}[x(n)]] \sim \mathcal{N}(\mu_{A_1}, \sigma^2_{A_1}), \quad (15)$$

where $\mu_{A_1} = A^2\Omega^2_{A_1}$, $\sigma^2_{A_1} = \Omega^2_{A_1}(\sigma^2_{V(A_1)} + \sigma^2_{U(A_1)}) + \sigma^2_w$, $\sigma^2_{U(A_1)} = \sigma^2_{V(A_1)} = 4\pi^2 f^2_{A_1} \sigma^2$, and $\sigma^2$ is the clock measurement error.

Referring to (14) and (15), the distribution of the mixed signal $E[\Psi_{ms}[x(n)]]$ is

$$E[\Psi_{ms}[x(n)]] = E[\Psi_{A_1}[x(n)]] + E[\Psi_{C_4}[x(n)]] \quad (16)$$
$$\sim \mathcal{N}(\mu_{ms}, \sigma^2_{ms}), \quad (17)$$

where $\mu_{ms} = \mu_{A_1} + \mu_{C_4}$ and $\sigma^2_{ms} = \sigma^2_{A_1} + \sigma^2_{C_4}$.

## V. Simulation

This section presents the performance of the proposed scheme and examines the impact of estimation errors on the correctness of signal reading.

### A. Performance Evaluation

Figures 7 and 8 investigate the system sensitivity to the AWGN measurement noise with synchronous clocking. As shown in Figure 7, given the measurement noise $w$ with the duration of segments $N = 5$, $\mu_w = 0$ and $\sigma_w = 0.01$, the proposed scheme can still distinguish the test signals very well. However, with a larger measurement noise $\sigma_w = 0.05$ (Figure 8), certain boundaries of the test signals are not distinguished obviously.

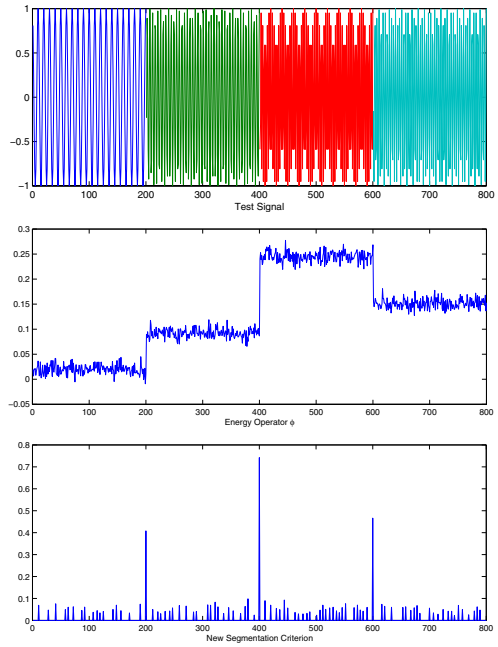


Fig. 7. Simulation example of segmentation of two channels with synchronous clocking and the measurement noise $\sigma_w = 0.01$.

Notice that a tradeoff exists in a good measure of frequency weighted energy and the desired duration of segments due to the noise level. Since for the non-linear energy operator only three samples (i.e. $x(n)$, $x(n-1)$, and $x(n-2)$ as described in (1)) are required to estimate the frequency weighted energy, therefore, determining appropriate window size is essential to generate the segmentation criterion based on the measurement noise. For instance, in Figure 9, the performance of the segmentation criterion with measurement noises $\sigma_w = 0.1$ and $N = 15$ is better than that of the segmentation criterion with measurement noises $\sigma_w = 0.1$ and $N = 5$. Thus, experimenting with the proposed approach, signals with more noise may require larger windows.

Figures 10 and 11 examine the impact of the precoding technique and channel effects. Without the pre-equalized TH-precoding technique, the channel effects and the measurement error of message transfer delay between two signals in $A_1$ and $C_4$ may degrade the system performance. Figure 10 shows the impact of the time synchronization error on signal segmentation. Observe that in Figure 10 the transition between two signals is not clear and the values of energy operator in transition areas are with large variation, which result in an inaccurate segmentation criterion. However, with the proposed TH precoding technique, Figure 11 illustrates typical runs of the received signal, the output of energy operator, and the segmentation criterion, which suggest that the test signal can be clearly segmented.

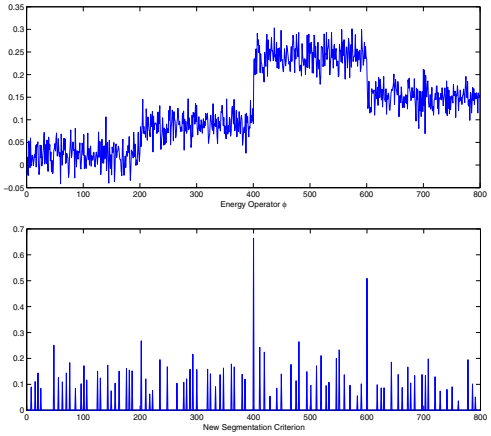


Fig. 8. Simulation example of segmentation of two channels with synchronous clocking and the measurement noise $\sigma_w = 0.05$.

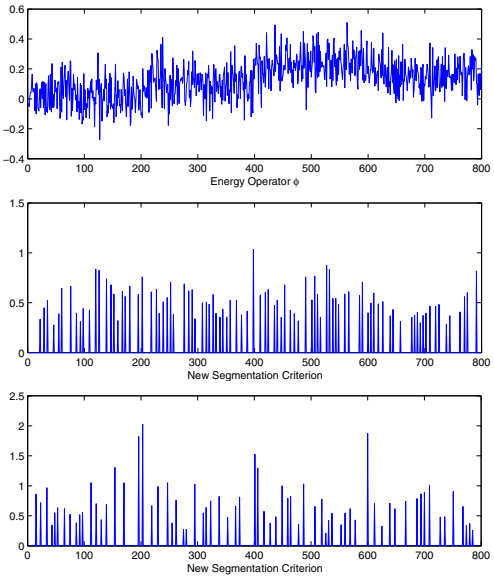


Fig. 9. Simulation example of segmentation of two channels with synchronous clocking and with measurement noises $\sigma_w = 0.1$ and $N = 5$ (top) and $N = 15$ (bottom), respectively.

### *B. Application: Wireless Sleep EEG System*

Since the variance of energy operator depends on the timing resolution, Figure 12 and 13 depict the corresponding energy output variances given the timing resolutions. As expected, in Figure 12 a higher timing resolution $\sigma$ (Phase I) introduces a lower variance of energy operator output $\sigma_{ms}$ (Phase II). Therefore, a lower timing resolution may increase the difficulty of distinguishing the boundaries of different EEG signal patterns. As shown in Figure 13, for a test signal composed of $f_1$ = 10 Hz and $f_2$ = 20 Hz, the timing resolution $\sigma$ = $10^{-6}$ second leads to $\sigma_{ms}$ = 0.0048 and $\sigma$ = $10^{-3}$ second leads to

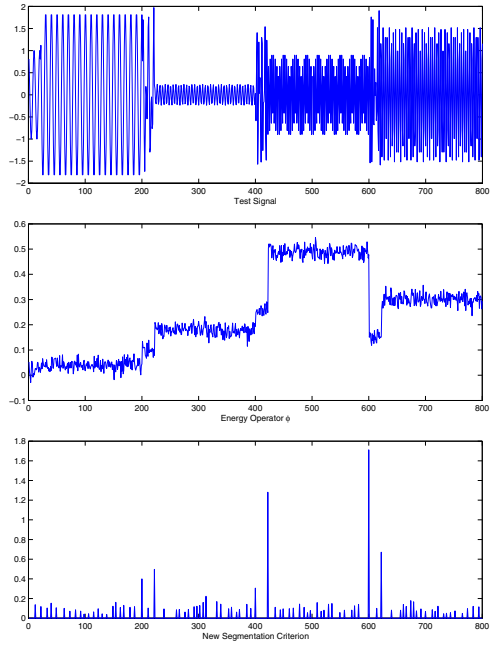


Fig. 10. The impact of the time synchronization error on signal segmentation without TH-Precoding.

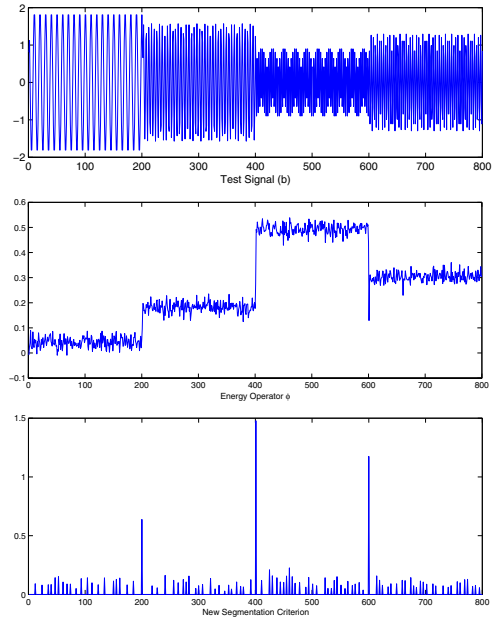


Fig. 11. The impact of the time synchronization error on signal segmentation with TH-Precoding.

$\sigma_{ms}$ = 0.477.

In Section V-A, the performance of the EEG segmentation algorithm is shown by a sine signal with immediate frequency

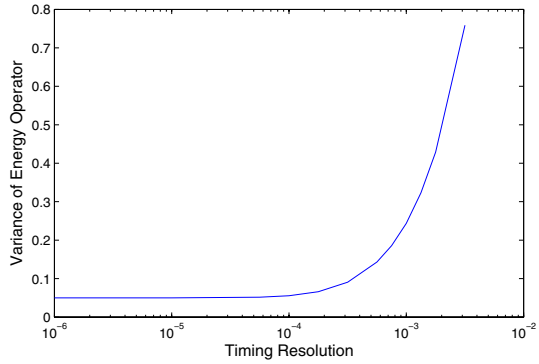


Fig. 12. The relationship between the timing resolution and the variance of the output of energy operator.

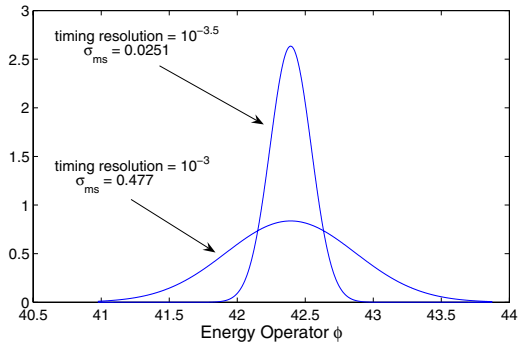


Fig. 13. The distribution of energy operator with varying the timing resolution.

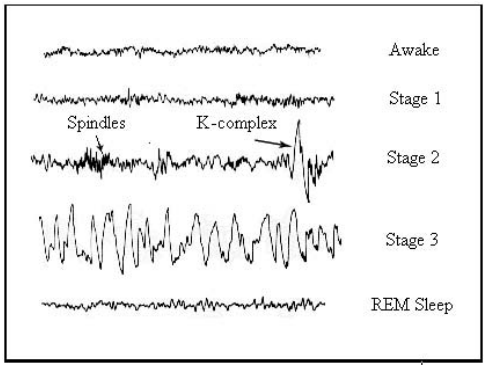


Fig. 14. Wave pattern of different sleep stages [23].

jumps. However, real EEG signals are composed of several frequencies at the same time (e.g. $\alpha$ waves 8-13 Hz, $\beta$ waves 14-30 Hz). For the sleep EEG measurement system, Figure 14 shows the wave pattern of different sleep stages [23]. In order to demonstrate the feasibility of the proposed method, simulation examples of sleep EEG signal segmentation are illustrated in Figures 15-17. In the experiment, the test signal consists of three wave patterns with the sampling frequency $f_s$=100 Hz. The first waveform is composed of combinations of two sine waves with $f_1$=10 Hz and $f_2$=18 Hz; the second waveform is composed of combinations of two sine waves with $f_1$=13 Hz and $f_2$=20 Hz; the third waveform is composed of combinations of two sine waves with $f_1$=10 Hz and $f_2$=15 Hz. Figure 15 shows a simulation example of signal segmentation with synchronous clocking and without measurement noises, which implies that the proposed scheme can govern the test signals very well.

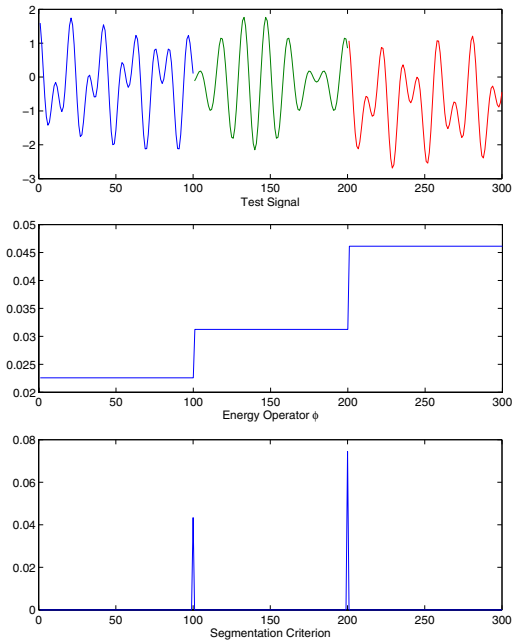


Fig. 15. Simulation example of signal segmentation with a test signal composed of three wave patterns.

Similar to the experimental results in Figures 10 and 11, the performance of signal segmentation with time synchronization error (Figure 16) produces a noisy segmentation criterion, whereas with the proposed scheme, the segmentation boundaries are obvious and the different wave patterns can be distinguished effectively (Figure 17).

## VI. Conclusion

This paper presents a method for collecting sleep EEG signals using cooperative communication and networking. The proposed decentralized method is applied to simultaneously undertake synchronization and propagation time estimation. Moreover, different EEG patterns are distinguished by the signal segmentation criterion using the dominant signal rhythms. Based on the proposed scheme, the impact of time synchronization on the diagnosis of EEG signals is investigated, which suggests that the wireless sensor nodes may make EEG detecting more authentic, especially for sleep EEG, since the

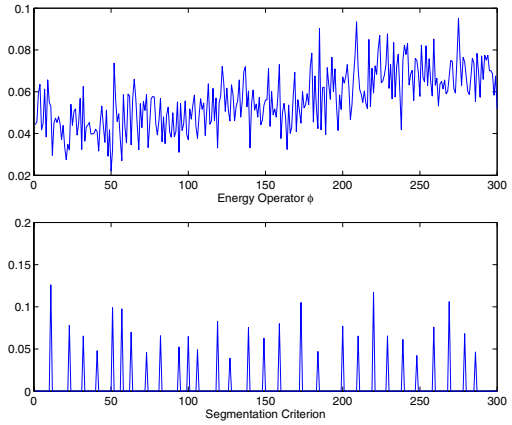


Fig. 16. Simulation example of segmentation of two channels with timing resolution $\sigma = 10^{-3}$ second, measurement noises $\sigma_w = 0.05$, and time synchronization error $20/f_s$, where $f_s = 100$ Hz.

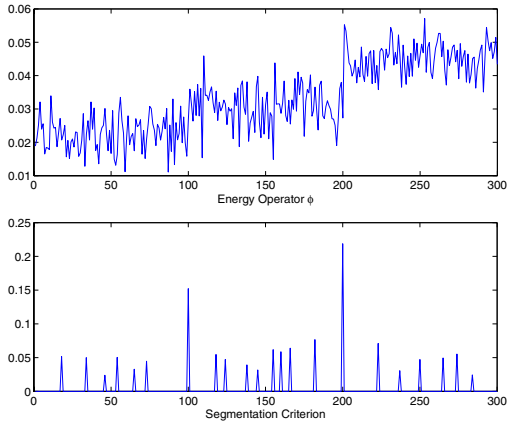


Fig. 17. Simulation example of segmentation of two channels with TH precoding and the measurement noise $\sigma_w = 0.05$.

proposed scheme may be applied to analyze the long time recording data efficiently. Compared with conventional EEG measurement systems, the proposed algorithm may provide a reliable EEG reading system with asynchronous pervasive sensing.

For the proposed measurement solution, trade-offs are found between model complexity, energy consumption, signal segmentation strategy, and sensible model description in real systems. Future plans will involve generalizing the methods to consider different EEG signal segmentation algorithms (e.g. wavelets) and to perform actual measurements to determine how precise the synchronization of EEG channels needs to be in practice.

## REFERENCES

[1] Joseph J. Carr and John M. Brown, "Instrumentation for Measuring Brain function," in *Introduction to Biomedical Equipment Technology*, Fourth Edition, pp. 369-395, 2001.

[2] D. Holschneider and A. Leuchter, "Clinical neurophysiology using electroencephalography in geriatric psychiatry: neurobiologic implication and clinical utility," in *J. Geriatr. Psychiatry Neurol.*, vol. 12, pp. 150-164, 1999.

[3] Halit Eren, "Instruments and Instrumentation," in *Wireless Sensors and Instruments Network, Design, and Application*, pp. 1-58, 2005.

[4] Robert Lin, Ren-Guey Lee, Chwan-Lu Tseng, Yan-Fa Wu and Joe-Air Jiang, "Design and Implementation of Wireless Multichannel EEG Recording System and Study of EEG clustering Methods," in *Biomedical Engineering Application, Basis & Communications*, pp. 276-283, 2006.

[5] Sharon A. Keenan, "An Overview of Polysomnography," in Christian Guilleminault ed., *Clinical Neurophysiology of Sleep Disorders*, pp. 33-50, 2005.

[6] M. Chen, J.-M. Lei, C.-L. Peng, and X.-M. Guo, "Time Synchronization in Wireless Physiological Information Sensor Network," in *Proc. IEEE Engineering in Medicine and Biology 27th Annual Cinference*, pp. 5176-5178, 2005.

[7] Ng et al, United State Patent (Patent No.: US 6,496,705), December 2002.

[8] Mehmet Engine, Tayfun Dalbasti, Merih Gulduren, Eray Davash and Erkan Zeki Engin, "A prototype portable system for EEG measurements," in *Measurement*, vol. 40, pp. 936-942, 2007.

[9] N. Golmie , D. Cypher and O. Rebala, "Performance analysis of low rate wireless technologies for medical applications," in *Computer Communication*, vol. 28, pp. 1266-1275, 2005.

[10] Behcet Sarikaya, M. Abdul and Siamak Rezaei, "Integrating Wireless EEGs into Medical Sensor Networks,"in *Proc. IEEE IWCMC*, pp. 1369-1373, 2006.

[11] C.-Y. Wen, R. D. Morris, and W. A. Sethares, "Distance Estimation Using Bidirectional Communications Without Synchronous Clocking," in *IEEE Transactions on Signal Processing*, vol. 55, pp. 1927-1939, May 2007.

[12] M. Tomlinson, "New Automatic Equalisier Employing Modulo Arithematic," in *Electronics Letters*, pp. 138-139, March 1971.

[13] C.-Y. Wen, J.-K. Chen, and W. A. Sethares, "Asynchronous Two-Way Ranging Using Tomlinson-Harashima Precoding and UWB Signaling," in *EURASIP Journal on Wireless Communications and Networking*, vol. 8, no. 3, pp. 1-13, 2008.

[14] J. F. Kaiser, "On a simple algorithm to calculate the 'energy' of a signal," in *Proc. IEEE Intl Conf. Acoust., Speech, and Signal Processing*, 1990.

[15] R. Agarwal and J. Gotman, "Adaptive segmentation of electroencephalographic data using nonlinear energy operator," in *Proc. IEEE ISCAS*, pp. 199-202, 1999.

[16] V. H. Poor, *An Introduction to Signal Detection and Estimation*, 2nd ed. New York: Springer-Verlag, 1994.

[17] W. S. Burdic, *Radar Signal Analysis*, Prentice-Hall, 1968.

[18] G. R. Curry, *Radar System Performance Modeling*, 2nd ed., Artech House, 2005.

[19] E.C. Fieller, "The Distribution of the Index in a Normal Bivariate Population," *Biometrika*, vol. 24, pp. 428-440, 1932.

[20] D.V. Hinkley, "On the Ratio of Two Correlated Normal Random Variables," *Biometrika*, vol. 56, pp. 635-639, 1969.

[21] R. Ware and F. Lad, "Approximating the Distribution for Sum of Product of Normal Variables," the research report of the Mathematics and Statistics department at Canterbury University, 2003.

[22] S. Gezici, Z. Tian, et al., "Localization via Ultra-Wideband Radios," in *IEEE Signal Processing Magazine*, vol. 22, no. 4, pp. 70-84, July 2005.

[23] K. Susmakova, 'Human Sleep and Sleep EEG," *Measurement Science Review*, vol. 4, pp. 59-74, 2004.